LINEAR PROPORTIONAL-INTEGRAL CONTROL OF TURBULENT CHANNEL FLOW FOR DRAG REDUCTION

Euiyoung Kim
School of Mechanical and Aerospace Engineering
Seoul National University
Seoul 151-744, KOREA
eykim03@snu.ac.kr

Haecheon Choi
School of Mechanical and Aerospace Engineering
Seoul National University
Seoul 151-744, KOREA
choi@snu.ac.kr

ABSTRACT

Choi, Moin and Kim (1994) applied the opposition control, $v_w = -v_{y_s^+ \approx 10}$, to turbulent channel flow and obtained about 25 % drag reduction, where v_w is the blowing and suction at the wall, and v is the wall-normal velocity, and y_s is the sensing location above the wall. From the classical control theory, the opposition control by Choi et al. (1994) is a proportional (P) control with a fixed feedback gain. In the present study, we investigate the performance of proportional-integral (PI) control in reducing the skin friction in a turbulent channel flow. The PI control is defined as $v_w = -\alpha\ v_{y_s} - \beta \int v_{y_s} dt$, where α and β are the proportional and integral feedback gains, respectively. The direct numerical simulation (DNS) and linear systems approach are conducted. In the effective sensing region, the PI control results in slightly more drag reduction and lower transient energy growth rate than the P control. The sensing velocity fluctuations, considered as an error in the control, approach zero with the PI control, while they do not go to zero with the P control.

INTRODUCTION

Control of turbulent flows, in particular the skin-friction reduction in a turbulent boundary layer, has attracted many researchers due to the high potential benefits. Various flow control strategies (active vs. passive; open-loop vs. closed-loop, etc.) have been developed and implemented over the years, and some of them were quite successful in achieving certain control objectives (Gad-el-Hak, 2000; Kim, 2003; Collins, 2004; Kim and Bewley, 2007; Choi et al., 2008).

Choi, Moin and Kim (1994) applied the opposition control (Fig. 1) to turbulent channel flow and obtained about 25 % drag reduction. The blowing and suction at the wall (v_w) is given as

$$v_w(x,z,t) = -v_{y_s}(x,z,t), \tag{1}$$

where v_{y_s} is the wall-normal velocity at the sensing location y_s. The idea in that study was to attenuate the strength of near-wall streamwise votices by providing a distributed blowing/suction at the wall, opposite to the motion induced by these vortices. From the classical control theory, the opposition control is a proportional (P) control with a fixed feedback gain, $\alpha = -1$. The P control is simple and easy to apply, but its result is quite sensitive to the sensing location y_s (Choi et al., 1994; Hammond et al., 1998) and feedback gain (Chung and Talha, 2011). Furthermore, the P control allows steady-state error, and thus the target sensing velocity fluctuations do not vanish. By adopting the integral (I) control, the proportional-integral (PI) control may remove the steady-state error, and result in more drag reduction.

Although turbulent flows are generally governed by nonlinear dynamics, linear systems approaches are useful to analyze and design the control method. This is because a linear mechanism plays a key role in maintaining near-wall turbulence structures responsible for high skin-friction drag in a turbulent boundary layer (Kim and Lim, 2000; Kim and Bewley, 2007), and thus a successful control aiming at altering the linear mechanism may yield significant changes in a turbulent boundary layer (Farrell and Ioannou, 1996; Lim and Kim, 2004).

In the present study, we apply the PI control to turbulent channel flow for drag reduction. We conduct direct numerical simulation of turbulent channel flow and linear systems approach, to evaluate the performance of PI control.

NUMERICAL METHODS FOR DNS

The governing equations for the unsteady incompressible viscous flow are given as

$$\frac{\partial u_i}{\partial t} + \frac{\partial u_i u_j}{\partial x_j} = -\frac{\partial p}{\partial x_i} + \frac{1}{Re}\frac{\partial^2 u_i}{\partial x_j \partial x_j}, \tag{2}$$

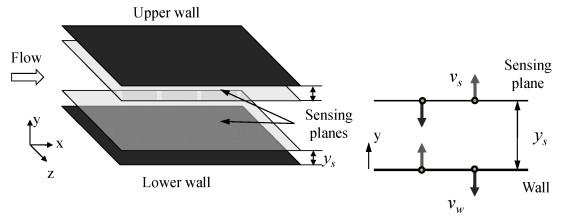

Figure 1. Schematic diagram of the opposition control by Choi et al. (1994).

$$\frac{\partial u_i}{\partial x_i} = 0, \tag{3}$$

where x_i's are the cartesian coordinates, u_i's are the corresponding velocity components, and p is the pressure. All variables are non-dimensionalized by the channel half-height (δ) and laminar centerline velocity (u_l). The Reynolds number considered is $Re = u_l\delta/\nu = 3000$ ($Re_\tau = u_\tau\delta/\nu \approx 140$, where u_τ is the wall-shear velocity). A constant mass flux is imposed throughout the computation.

A second-order semi-implicit fractional step method is used in time, and a second-order central difference scheme is used in space. The periodic boundary conditions are used in the streamwise and spanwise directions, and the no-slip condition is applied to both the upper and lower walls. The computational domain size is $3\pi\delta(x) \times 2\delta(y) \times \pi\delta(z)$ and the number of grid points is $64(x) \times 65(y) \times 64(z)$. Uniform grids are used in the streamwise and spanwise directions, while non-uniform grids are used in the wall-normal direction. The grid spacings in wall unit are $\Delta x^+ \approx 20$, $\Delta y^+_{min} \approx 0.45$, $\Delta z^+ \approx 6.6$, respectively.

During the control, all conditions are kept the same as in the the simulation without control except for the boundary conditions at the wall on which the control strategies are implemented. At each instant the boundary condition is defined as

$$v_w(x,z,t) = -\alpha v_{y_s}(x,z,t) - \beta \int v_{y_s}(x,z,t)dt, \tag{4}$$

where α and β are the proportional and integral feedback gains, respectively. The skin-friction reduction is determined from the change in the mean pressure gradient necessary to drive the flow at a constant mass flow rate.

LINEAR SYSTEMS APPROACH

We use the collocation matrix approach used by Bewley and Liu (1998). The linearized Navier-Stokes equations with control output can be written in the following state-space representation:

$$\dot{\mathbf{x}} = \mathbf{A}\mathbf{x} + \mathbf{B}\mathbf{u}, \tag{5}$$

$$\mathbf{y} = \mathbf{C}\mathbf{x}. \tag{6}$$

Here, the vector $\mathbf{x}$ represents the state of the system, and it consists of the wall-normal velocity (v) and vorticity (ω) at each collocation point. The dot denotes time derivative. The vector $\mathbf{u}$ is the input vector that represents the blowing and suction at the wall.

The operator $\mathbf{A}$ represents the linearized Navier-Stokes system defined as

$$\mathbf{A} = \begin{bmatrix} L_{os} & 0 \\ L_c & L_{sq} \end{bmatrix}. \tag{7}$$

Here, L_{os}, L_{sq} and L_c represent the Orr-Sommerfeld, Squire and linear coupling operators, respectively, and are defined as

$$L_{os} = \Delta^{-1}(-ik_xU\Delta + ik_xU'' + \frac{1}{Re_\tau}\Delta^2), \tag{8}$$

$$L_{sq} = -ik_xU + \frac{1}{Re_\tau}\Delta, \tag{9}$$

$$L_c = ik_zU'. \tag{10}$$

Here, k_x and k_z are the streamwise and spanwise wave numbers, respectively, $\Delta = \partial^2/\partial y^2 - k_x^2 - k_z^2$, U is the mean velocity, and prime denotes $\partial/\partial y$. The Reynolds number in the linear system approach is taken to be $Re_\tau = u_\tau\delta/\nu = 180$. The vector $\mathbf{y}$ is the output vector, which is the wall-normal velocity at the sensing location. The observation operator $\mathbf{C}$ is constructed once the sensing location y_s is chosen.

With the P control, the control input is given as $\mathbf{u} = -\alpha\mathbf{y} = -\alpha\mathbf{C}\mathbf{x}$. By substituting this into Eq. (5), the system equation for the P control becomes

$$\dot{\mathbf{x}} = (\mathbf{A} - \alpha\mathbf{B}\mathbf{C})\mathbf{x}. \tag{11}$$

On the other hand, for the PI control, we introduce the vector $\mathbf{z}$ satisfying $\dot{\mathbf{z}} = \mathbf{y} = \mathbf{C}\mathbf{x}$. Then the input vector becomes $\mathbf{u} = -\alpha\mathbf{y} - \beta\mathbf{z}$. By substituting this into Eq. (5), the system equation for the PI control is given as

$$\begin{bmatrix} \dot{\mathbf{x}} \\ \dot{\mathbf{z}} \end{bmatrix} = \begin{bmatrix} \mathbf{A} - \alpha\mathbf{B}\mathbf{C} & -\beta\mathbf{B} \\ \mathbf{C} & \mathbf{0} \end{bmatrix} \begin{bmatrix} \mathbf{x} \\ \mathbf{z} \end{bmatrix}. \tag{12}$$

The solutions for the P and PI controls are then expressed as

$$\mathbf{x}(t) = \mathbf{X}\exp(\Lambda t)\mathbf{X}^{-1}\mathbf{x}(0), \tag{13}$$

where $\mathbf{X}$ is the eigenvector matrix of the system matrix in Eq. (11) or Eq. (12) for the P or PI control, respectively, and Λ is the eigenvalue matrix whose diagonal terms $\lambda_{\kappa\kappa}$ are the eigenvalues of the system matrix.

To analyze the transient energy growth, we consider the growth ratio function defined as the ratio of the kinetic energy of a disturbance (E) at a given time to that at $t = 0$:

$$G(t) = \frac{E(t)}{E(0)}, \tag{14}$$

where

$$E \equiv \int_{-1}^{1} \left[v^* v + \frac{1}{k_x^2 + k_z^2} \left(\frac{\partial v^*}{\partial y} \frac{\partial v}{\partial y} + \omega^* \omega \right) \right] \mathrm{d}y. \tag{15}$$

The quantity E is expressed as $E(t) = \mathbf{x}^*(t)\mathbf{Q}\mathbf{x}(t)$, where the matrix $\mathbf{Q}$ is defined in terms of an inner product in discrete space. The superscript $*$ denotes the Hermitian conjugate. The matrix $\mathbf{Q}$ is further decomposed in the form of $\mathbf{Q} = \mathbf{F}^*\mathbf{F}$. Then,

$$E(t) = \mathbf{x}^*(t)\mathbf{F}^*\mathbf{F}\mathbf{x}(t) = \|\mathbf{F}\mathbf{x}(t)\|_2^2 = \|\mathbf{F}\mathbf{X}\exp(\Lambda t)\mathbf{X}^{-1}\mathbf{x}(0)\|_2^2, \tag{16}$$

where $\| \bullet \|_2$ represents the 2-norm (Euclidian norm). Combining Eqs. (14) and (16), we obtain the growth ratio at t as

$$G(t) = \frac{\|\mathbf{F}\mathbf{X}\exp(\Lambda t)\mathbf{X}^{-1}\mathbf{x}(0)\|_2^2}{\|\mathbf{F}\mathbf{x}(0)\|_2^2} = \|\mathbf{F}\mathbf{X}\exp(\Lambda t)\mathbf{X}^{-1}\mathbf{F}^{-1}\|_2^2. \tag{17}$$

The 2-norm of a matrix can be easily computed from the singular value decomposition (SVD) of the matrix. Typical SVD provides a diagonal matrix Σ and two orthogonal matrices $\mathbf{U}$ and $\mathbf{V}$ such that $\mathbf{A} = \mathbf{U}\Sigma\mathbf{V}^*$. The column vectors of $\mathbf{V}$ and $\mathbf{U}$ are referred to as right and left singular vectors, respectively. The diagonal elements of Σ are the singular values (σ's), which represent the two-norm ratios of corresponding column vectors of $\mathbf{V}$ and $\mathbf{U}$. The largest value of σ^2 represents the maximum energy growth ratio at t, and the corresponding column vectors of $\mathbf{U}$ and $\mathbf{V}$ are the flow field at t and the initial flow field, respectively. In the following section, we apply the SVD analysis to the channel flow system with the P and PI controls. By comparing the largest singular values for the energy growth ratio for different control parameters, we evaluate the performances of the P and PI controls.

RESULTS AND DISCUSSION

Direct Numerical Simulation

Fig. 2 shows the variations of drag for the P and I controls with varying the control parameters. The drag variation (ΔD) is defined as

$$\Delta D(\%) = \frac{D_{control} - D_{no\ control}}{D_{no\ control}} \times 100. \tag{18}$$

As y_s increases, the drag decreases, reaches minimum and then increases more than that of no control for both P and I controls. With the controls, the drag reduction occurs in a different range of sensing location depending on the control

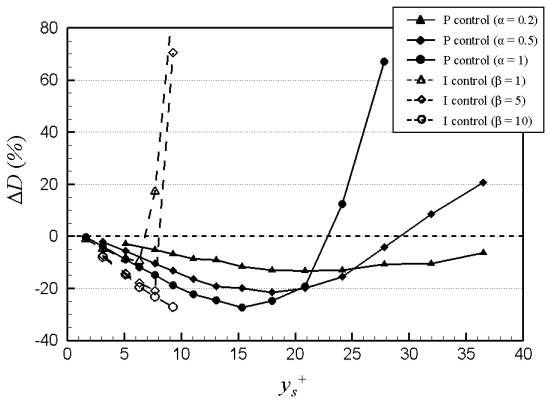

Figure 2. Drag variation for the P and I controls.

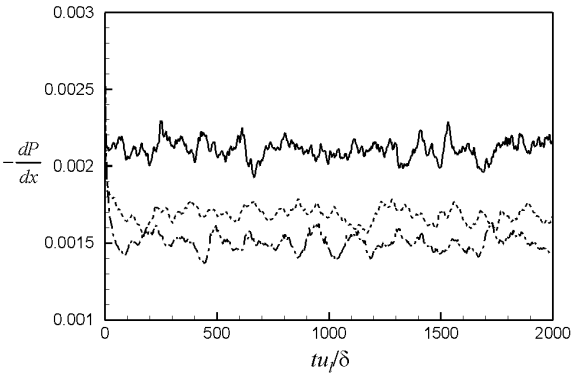

Figure 3. Time histories of the mean pressure gradient required to drive a constant mass flow rate: ——, no control; - - -, P control ($\alpha = 1$); – - –, PI control ($\alpha = 1$, $\beta = 10$). $y_s^+ = 9.3$ for the P and PI controls.

parameters. Overall, the effective sensing region for I control is narrower than that for the P control, and the maximum amount of drag reduction is almost same for the both controls. This result indicates that the P control alone is better than the I control alone.

From this result, we add the I control to the P control of $\alpha = 1$ to investigate the performance of the PI control. Fig. 3 shows the time history of the mean pressure gradient required to drive a constant mass flow rate for the PI control, together with those of no control and the P control. With the PI control ($\alpha = 1$, $\beta = 10$), we obtain nearly 30 % drag reduction which is 10 % more reduction than that of the P control.

Turbulence intensities for the controlled flows are shown in Fig. 4. Turbulence intensities are significantly reduced and shift outwards by the controls. In our PI or P control, the wall-normal velocity fluctuations at the sensing location are the error. With the P control, these velocity fluctuations at the sensing location are significantly reduced, but they are not zero. On the other hand, with the PI control, v_{rms} becomes nearly zero at the sensing location, as expected from the role of the I control.

The contours of instantaneous streamwise vorticity in a

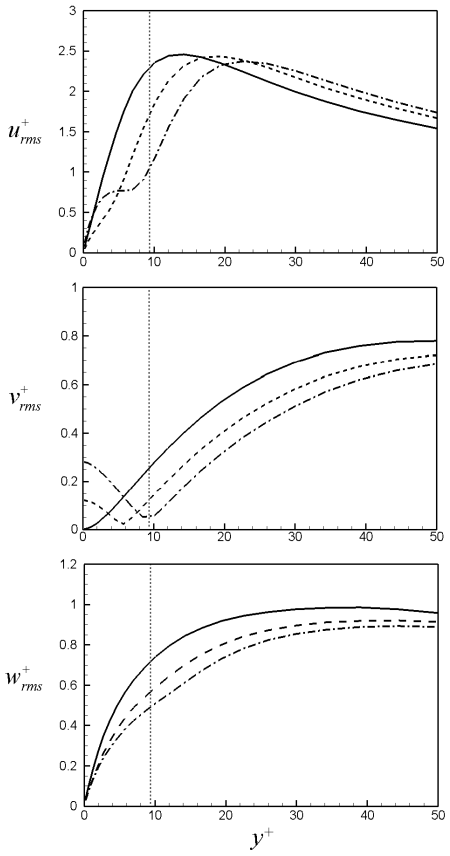

Figure 4. Root-mean-square velocity fluctuations normalized by the wall-shear velocity: ——, no control; - - -, P control ($\alpha = 1$); – – –, PI control ($\alpha = 1, \beta = 10$). $y_s^+ = 9.3$ for the P and PI controls. The dotted vertical line denotes the sensing location.

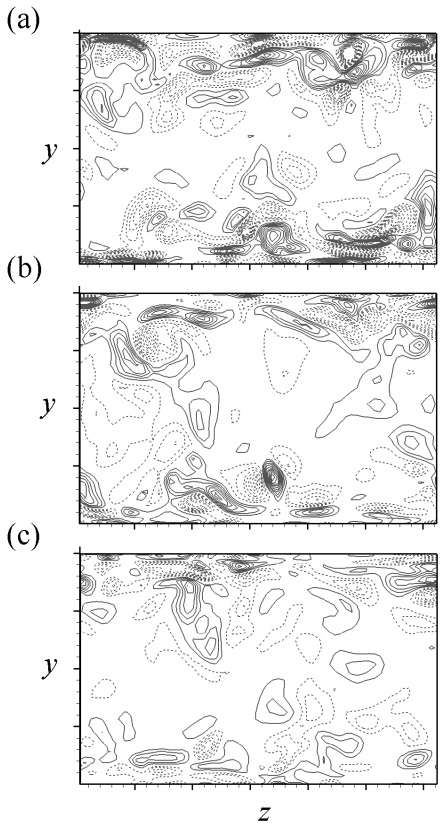

Figure 5. Contours of the instantaneous streamwise vorticity in a cross plane: (a) no control; (b) P control ($\alpha = 1$); (c) PI control ($\alpha = 1$, $\beta = 10$). $y_s^+ = 9.3$ for the P and PI controls. The contour levels range from $\omega_x \delta / u_l = -2$ to 2 by increments of 0.2. Dotted contours indicate negative values.

yz-plane are shown in Fig. 5. The feedback controls significantly reduce the strength of the streamwise vorticity in the wall region. Fig. 6 shows the energy spectra of the sensing velocity. With the P control, the sensing velocity fluctuations of all the frequency range are reduced. With the PI control, on the other hand, the energy at the low frequency range is reduced significantly possibly owing to the role of the I component. However, the PI control does not reduce the energy at high frequencies.

SVD Anaysis

In this section, we discuss the results from the SVD analysis. Fig. 7 shows the first 10 singular values representing the biggest disturbance energy growth ratios for two different wavenumber sets. We use the eddy turnover time in the near-wall region, $t^+ = 80$, which resulted in the optimal disturbance similar to those observed in turbulent boundary layers (Butler and Farrell, 1993). The wavenumber set, $k_x = 0$ and $k_z = 10.5$, represents the case of maximum $G(t)$ without control (Figs. 7 (a) and (b)). The largest singular value indicating $G(t)$ is reduced with both the P and PI controls at $y_s^+ = 10.4$, whereas it increases for the PI control and decreases for the P control at $y_s^+ = 15.2$. On the other hand, for the wavenumber set $k_x = 2.6$ and $k_z = 0.0$ (Figs. 7 (c) and (d)), both controls increase the singular values, meaning that the transient energy at this wavenumber set increases with both controls.

The contours of $G(t)$ for all wave-number pairs are plotted in Fig. 8. Without control (the top figures), the maximum $G(t)$ occurs at $k_x = 0$ and $k_z = 10.5$. The corresponding spanwise wavelength is $l_z^+ \approx 110$, which is approximately equal to the wall-layer streak spacing. The maximum value of $G(t)$ decreases for the P control at $y_s^+ < 15$, and for the PI control at $y_s^+ < 13$. At higher y_s, $G(t)$ increases drastically. The maximum $G(t)$ occurs on the $k_z = 0$ axis when y_s is large.

The results from the present SVD analysis agree well with the DNS results: (1) when y_s is within the effective range, the transient energy growth rate from SVD and the skin friction from DNS are reduced; (2) when y_s is large, both of them increase; (3) the PI control shows more drag reduction than the P control when y_s is very near the wall, as decrease for the growth rate; (4) according to the control theory, the I control eliminates the steady-state error that occurs with the P control, but the I control may cause an overshot of the set-point value and often make the system less stable. Hence, rapid increases of the drag and growth rate occur at high y_s's.

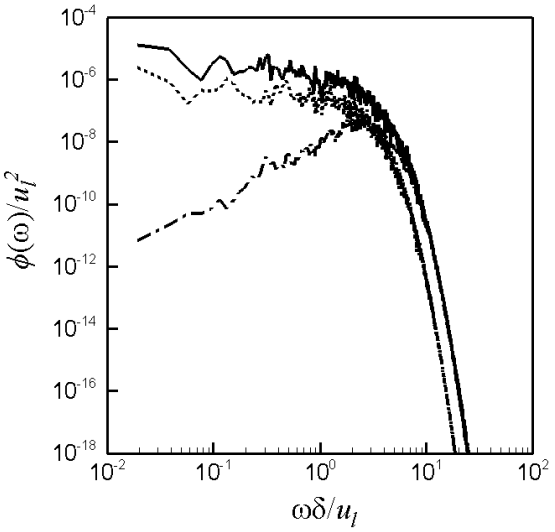

Figure 6. Frequency spectra of the sensing velocity: ——, no control; - - -, P control ($\alpha = 1$); – - –, PI control ($\alpha = 1$, $\beta = 10$). $y_s^+ = 9.3$ for the P and PI controls.

CONCLUSIONS

In the present study, we investigated the performance of the linear proportional-integral control for the drag reduction of turbulent channel flow by direct numerical simulation and linear systems approach. In both approaches, the PI control showed better performance than the P control in the effective sensing region. The wall-normal velocity fluctuations at sensing location, which is considered as an error in the control theory, became zero, whereas those with P control did not. Especially, the PI control significantly reduced the low-frequency components of the sensing velocity fluctuations. However, when y_s was located outside the effective sensing region, the I control rapidly increased both the drag in turbulent channel flow and the transient energy growth rate in linear system.

ACKNOWLEDGMENTS

This work is supported by the WCU, CRC and Priority Research Centers Programs through NRF, MEST, Korea.

REFERENCES

Bewley, T. R., and Liu, S., 1998, "Optimal and robust control and estimation of linear paths to transition", J. Fluid Mech., vol. 365, pp. 305-349.

Butler, K. M., and Farrell, B. F., 1993, "Optimal perturbations and streak spacing in wall-bounded turbulent shear flow", Phys. Fluids A, vol. 5, pp. 774-777.

Choi, H., Jeon, W.-P., and Kim, J., 2008, "Control of flow over a bluff body", Annu. Rev. Fluid Mech., vol. 40, pp. 113-139.

Choi, H., Moin, P., and Kim, J., 1994, "Active turbulence control for drag reduction in wall-bounded flows", J. Fluid Mech., vol. 262, pp. 75-110.

Chung, Y. M., and Talha, T., 2011, "Effectiveness of active flow control for turbulent skin friction drag reduction", Phys. Fluids, Vol. 23, 025102.

Collis, S. S., Joslin, R. D., Seifert, A., and Theofilis, V., 2004, "Issues in active flow control: theory, control, simulation, and experiment", Progress in Aerospace Sciences, Vol. 40, pp. 237-289.

Farrell, B. F., and Ioannou, P. J., 1996, "Turbulence suppression by active control", Phys. Fluids, Vol. 8, pp. 1257-1268.

Gad-el-Hak, M., 2000, "Flow Control: Passive, Active, and Reactive Flow Management", Cambridge, Cambridge Univ. Press, UK.

Hammond, E. P., Bewley, T. R., and Moin, P., 1998, "Observed mechanisms for turbulence attenuation and enhancement in opposition-controlled wall-bounded flows", Phys. Fluids, Vol. 10, pp. 2421-2423.

Kim, J., 2003, "Control of turbulent boundary layers", Phys. Fluids, Vol. 15, pp. 1093-1105.

Kim, J., and Bewley, T. R., 2007, "A linear systems approach to flow control", Annu. Rev. Fluid Mech., vol. 39, pp. 383-417.

Kim, J., and Lim, J., 2000, "A linear process in wall-bounded turbulent shear flows", Phys. Fluids, Vol. 12, pp. 1885-1888.

Lim, J., and Kim, J., 2004, "A singular value analysis of boundary layer control", Phys. Fluids, vol. 16, pp. 1980-1988.

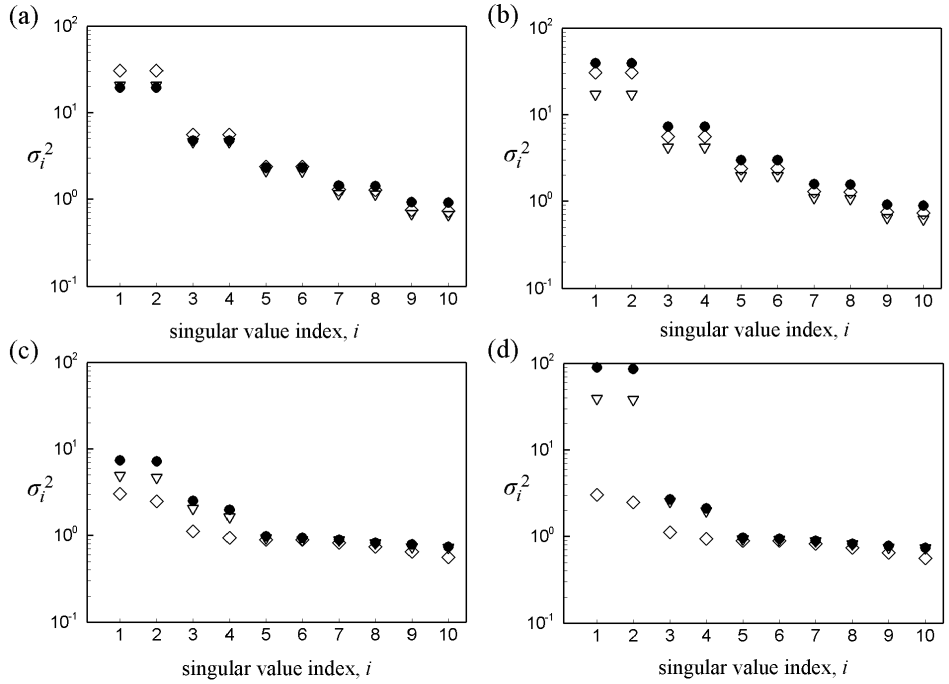

Figure 7. First 10 singular values for $\diamondsuit$, no control; $\bigtriangledown$, P control ($\alpha = 1$); $\bullet$, PI control ($\alpha = 1$, $\beta = 10$) at $t^+ = 80$: (a) $k_x = 0$, $k_z = 10.5$ and $y_s^+ = 10.4$; (b) $k_x = 0$, $k_z = 10.5$ and $y_s^+ = 15.2$; (c) $k_x = 2.6$, $k_z = 0$ and $y_s^+ = 10.4$; (d) $k_x = 2.6$, $k_z = 0$ and $y_s^+ = 15.2$.

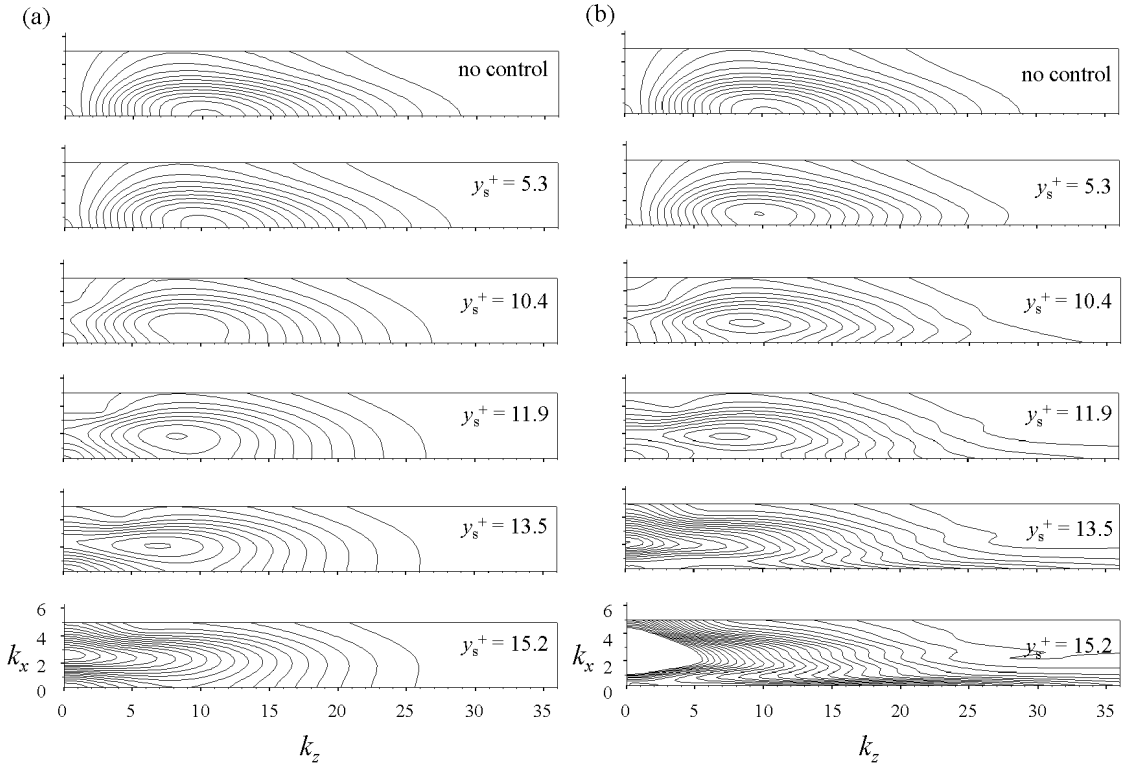

Figure 8. Contours of $G(t)$ at $t^+ = 80$ in the (k_x, k_z) plane for various sensing locations: (a) P control ($\alpha = 1$); (b) PI control ($\alpha = 1$, $\beta = 10$). The contour levels range from $G(t) = 0$ to 50 by increments of 2.